Desalination and Water Treatment
www.deswater.com

doi:10.5004/dwt.2017.20692

76 (2017) 112–120
May

Synthesis and characterization of silver decorated polysulfone/cellulose acetate hybrid ultrafiltration membranes using functionalized TiO_2 nanoparticles

Kola Sindhu Sri, Abhinav K. Nair, P.E. Jagadeesh Babu*

Department of Chemical Engineering, National Institute of Technology Karnataka, Surathkal, Mangalore 575 025, India, Tel. +91 9739330399, email: sssindhusri@gmail.com (S.S. Kola), Tel. +91 8792706002, email: abhinav2411@yahoo.com (A.K. Nair), Tel. +91 9632896086, Fax +91 08242474057, email: dr.jagadeesh@yahoo.co.in, jagadeesh78@nitk.ac.in (P.E. Jagadeesh Babu)

Received 10 September 2016; Accepted 9 March 2017

ABSTRACT

Amine functionalized TiO_2 nanoparticles were synthesized via surface reaction with 3-Aminopropyl triethoxysilane. These nanoparticles were added to polysulfone and cellulose acetate blend casting solutions in 1-Methyl-2-pyrrolidone to form hybrid membranes by phase inversion. The amine groups on the surface of the membranes were used as absorption sites for silver nanoparticles. The obtained membranes were characterized using Fourier Transform Infra Red spectroscopy, Scanning electron microscope and X-ray diffraction. Water uptake studies and contact angle measurements were done to evaluate hydrophilicity of the membranes. Pure water flux studies of the membrane were carried out in a dead end filtration unit. Rejection and antifouling studies were carried out using bovine serum albumin as a model protein. The hybrid membranes exhibited better permeability and fouling resistance. The hybrid membranes with silver decoration on the surface showed microbial resistance.

Keywords: Amine functionalized TiO_2; Polysulfone; Cellulose acetate; Hybrid; Silver nanoparticles

1. Introduction

The development of membranes with better permeate flux and improved antifouling properties are an intriguing field of research in membrane technology. Polysulfone (PSF) is common polymer material in the manufacture of asymmetric organic ultrafiltration membranes due to its good thermal, mechanical and chemical properties. Its use in water filtration is restricted due to its hydrophobicity, which results in greater fouling and subsequent water flux drop [1]. One could find in the literature several attempts to overcome the hydrophobicity of polysulfone. These include blending with hydrophilic polymers, addition of hydrophilic modifiers, surface treatment etc [2,3].

Cellulose acetate (CA) is a well known hydrophilic polymer used for synthesizing aqueous based membranes for ultrafiltration and reverse osmosis [4]. Being hydrophilic, CA is less susceptible to fouling. But it has less chemical resistance and poor mechanical properties. Blending polymers is an effective tool to combine diverse properties and to extract the best out of the both [5]. Hydrophilic and hydrophobic balance is essential for a membrane, the combination of PSF and CA should thus result in a synergistic effect in the resulting membrane. Researchers have reported blending these polymers and the composite membranes had enhanced performance [6,7].

Nanocomposite membranes have attracted much attention over the last decade; addition of small amounts of nanoscale additive could result in greater property enhancement. There have been several reports of polysulfone based nanocomposite membranes. Nanoadditives like carbon nanotubes, graphene oxide, nanoclay etc., have shown very good property enhancement [8–11]. Addition of inorganic nanoparticles like Al_2O_3, Fe_2O_3, SiO_2, TiO_2 etc., have also resulted in better hydrophilicity and antifouling properties. These inorganic nanoparticles are highly hydrophilic and thus impart hydrophilicity to the membrane

*Corresponding author.

surface. Improved hydrophilicity enables better interaction with water than the foulant, thus the membrane gains anti-fouling property [12–18].

Typically any additive in an ultrafiltration membrane should help in countering two types of fouling, membrane fouling caused by organic matter and bio-fouling. Among the various inorganic additives, TiO_2 nanomaterials have been proven to effectively enhance hydrophilicity and retard fouling due to organic pollutants in case of PSF [19,20]. But TiO_2 has bactericidal properties only under UV irradiation. Meanwhile, the incorporation of noble metal nanoparticles, particularly silver has interesting antimicrobial capabilities; it can inhibit biofouling and film formation [21]. In the present work we have attempted to extract the synergy of most methods reported to enhance the properties of PSF. Firstly PSF is blended with a hydrophilic polymer, CA. Secondly a nanohybrid membrane is developed using amine fuctionalised TiO_2 nanoparticles (ATNP). Lastly the amine groups on the surface of the TiO_2 nanoparticles are used as adsorption sites for Ag nanoparticles, decorating the membrane surface with Ag nanoparticles.

2. Experimental

2.1. Materials

3-Aminopropyl triethoxysilane (APTES), succinic anhydride, ethanol, isopropanol, polysulfone (average molecular number (M_n) ~16000), cellulose acetate (M_n ~30000), 1-Methyl-2-pyrrolidone (NMP), silver nitrate ($AgNO_3$), ethylene glycol and poly-vinyl-pyrrolidone (PVP) were purchased from Sigma-Aldrich Co, Bangalore, India. Dimethyl formamide (DMF), ammonium hydroxide (NH_4OH) and sodium hydroxide (NaOH) were purchased from Merck, India Ltd. Bovine serum albumin (BSA) was purchased from Himedia laboratories Pvt Ltd, India.

2.2. Preparation of amine functionalized titanium dioxide nanoparticles (ATNP)

ATNPs were synthesized using similar procedure reported in literature [22]. In brief, 0.4 g TiO_2 nanoparticles (TNP) were dispersed in 20 ml isopropanol, then 0.2 g of 3-aminopropyl triethoxysilane (APTES) and 10 ml of distilled water were added to the solution obtained. The resulting solution was stirred at room temperature for 48 h and the solution was dried at a temperature of 60ºC to remove the solvent.

2.3. Preparation of hybrid membranes

To obtain a homogeneous polymer solution, PSF (15 wt.%) and CA (5 wt.%) were dissolved in NMP (80 wt.%) and stirred for 4 h at a temperature of 100°C. Required amounts of ATNP as per Table 1, was added to the obtained solution, stirred for 30 min and sonicated for a time period of 30 min. After this, the resulting dispersion was again stirred for 30 min. This casting solution was casted on a glass plate using a polished glass rod. The glass plate was then immersed in distilled water at 20°C for 24 h before testing [5].

Table 1
Blending compositions of membranes

Membranes	Polymer solution(PS)			Additive	Additive : PS (wt./wt.) %
	PSf (wt.%)	CA (wt.%)	NMP (wt.%)	ATNP (wt.%)	
M-0	15.00	5.00	80.00	0.00	0
M-1	14.85	4.95	79.21	0.99	1
M-3	14.56	4.85	77.67	2.91	3
M-5	14.29	4.76	76.19	4.76	5
M-7	14.02	4.67	74.77	6.54	7
M-10	13.64	4.55	72.73	9.09	10
M-12	13.39	4.46	71.43	10.71	12

2.4. Preparation of silver decorated membranes

Silver decoration of the membrane surfaces was achieved via aminosilane coupling as a connecting bridge as reported by Lv et al. [23]. Firstly, silver nanoparticle suspension is synthesized. Two solutions of $AgNO_3$ and PVP were prepared by adding 0.017 g of $AgNO_3$ and 0.022 g of PVP to 10 ml ethylene glycol with subsequent stirring for 10 min. To the prepared PVP solution, $AgNO_3$ solution was added drop-wise and vigorously stirred at room temperature for 4 h. A reddish brown suspension was obtained. The prepared hybrid membranes were washed with ethanol and vacuum dried at 60°C for 2 h. Finally, these membranes were dipped in the above obtained silver nanoparticle suspension for a day. Bonding between membrane surface and Ag nanoparticles takes place via aminosilane groups of ATNP as shown in Fig. 1. Silver nanoparticle decorated membranes are thus obtained (Fig. 2). These membranes were washed with ethanol to remove all boundless particles from the surface and dried at 60°C.

3. Characterization

3.1. Transmission electron microscopy (TEM)

TEM (JEOL, JEM-2100) was used for analyzing the nanoparticles. Samples were prepared by depositing a drop of a well dispersed dilute nanoparticle suspension on to a carbon coated copper grid.

3.2. Fourier transform infra red (FT-IR) spectroscopy

The FT-IR spectra of membranes were obtained using Shimadzu FTIR- 8400S spectrometer in the range of 4000–400 cm^{-1}. Hybrid membranes and nanoparticles spectra were analyzed.

3.3. X-ray diffraction(XRD) analysis

X-ray diffraction was done using Goniometer (JEOL Dx-GE-2P, Japan), X-ray Diffractometer equipped with monochromatised high intensity Cu Kα radiation (λ = 1.54058 Å). The diffractograms were obtained at 0.16°/s in the 2θ range 10–60°.

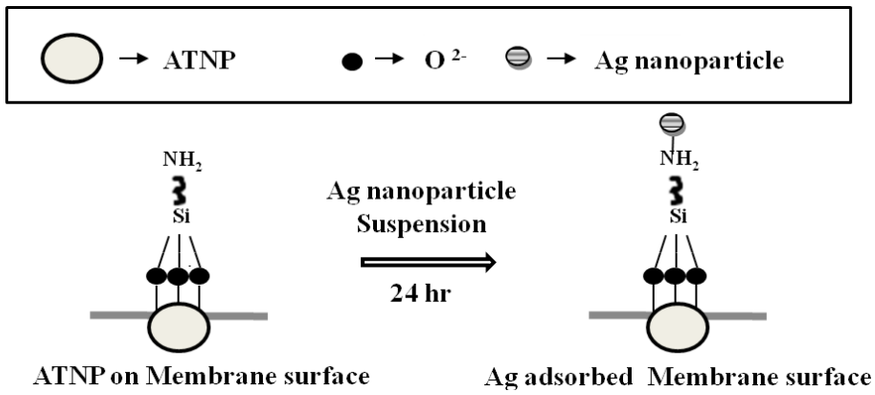

Fig. 1. Bonding between membrane surface and Ag nanoparticles via aminosilane group on ATNP.

Fig. 2. Silver decorated hybridM-12 membrane.

3.4. Ultra violet-visible (UV-Vis) Spectroscopy

Hitachi U-2900 Spectrophotometer with a wavelength range of 300–900 nm was used for the spectral study of the synthesized silver nanoparticles and also for the estimation of BSA concentrations.

3.5.Scanning electron microscopy(SEM)

Jeol JSM-6380LA analytical SEM was used to get SEM images of the nanoparticles and hybrid membranes. To get the cross sectional images of the hybrid membranes, they were cryogenically fractured using liquid nitrogen,before scanning each sample was gold sputtered. Elemental mapping of Ag on the Ag decorated membrane surface was also carried out.

3.6. Contact angle measurement

Contact angle of the membranes was calculated using sessile droplet method in FTA-200 Dynamic contact angle analyzer. Values of three different locations were considered to reduce experimental error.

3.7. Permeation properties

Sterlitech HP4750 stirred cell dead end filtration unit with an effective membrane area of 14.6 cm^2 was used for conducting the permeation studies of the membranes. Membranes were kept submerged in distilled water for a day prior to flux study. The time dependent variations in pure water flux (PWF) of membrane were calculated. The permeate collection was initiated following 25 min of pressurizing at 0.3 MPa transmembrane pressure (TMP) at 25°C. Samples were collected at each 5 min intermission. The PWF (J_w) was estimated using the following equation:

$$J_w = \frac{Q}{\Delta t\, A} \tag{1}$$

where J_w is expressed in L/m^2h and Q is the amount of water collected for Δt (h) time duration using a membrane of area A (m^2).

3.8. Antifouling properties

The antifouling properties of the membrane were determined as reported in literature [24]. In short, original PWF of the membrane J_{w1} (L/m^2h) was estimated at 0.2 MPa TMP. The antifouling property of the membranes was determined using BSA as standard protein for rejection. 0.4 g of BSA was dissolved in 500 mL of distilled water to give an aqueous solution which was then filtered through the membrane for a duration of 90 min. Later on the membrane was washed with distilled water for 30 min and again the pure water flux J_{w2} (L/m^2h) was obtained. The membranes antifouling properties were evaluated in terms of flux recovery ratio (FRR) using the following correlation:

$$FRR(\%) = \frac{J_{w2}}{J_{w1}} \times 100 \tag{2}$$

In order to establish the rejection of the membrane, the permeate solution samples were collected. 0.1 ml of the collected sample was added to 3 ml of Bradford reagent and

left for 10 min, and then it was analyzed using UV-spectrometer. The percentage BSA rejection (R%) was calculated using the following correlation:

$$R\% = \left(1 - \frac{C_p}{C_f}\right) \times 100 \quad (3)$$

where C_p (mg/mL) and C_f(mg/mL) are the BSA concentrations in permeate and feed respectively. The concentrations were calculated at a wavelength of 595 nm using UV-Vis spectroscopy.

3.9. Antibacterial properties

Zone of inhibition technique was used to verify the antibacterial properties of the hybrid membrane [23]. Nutrient agar solution was prepared by adding 9.2 g of nutrient agar in 300 ml of distilled water. To determine the zone of inhibition, nutrient agar was poured onto sterilized petridish and left for sometime at room temperature to solidify. Then 100 µL of bacterial water (1 inoculation loop) containing *Escherichia coli* (*E. coli*) bacteria was streaked over the petridish and spread uniformly throughout. A small circular piece of membrane was placed over the solidified agar gel at the centre in the petridish and this plate was placed in the incubator for 24 h at 37ºC. After one day of incubation, the zone of inhibition was observed.

In order to assess the antibacterial properties of the membrane in liquid media the following method was used. 50 mL Luria-Bertani broth was prepared in three conical flasks. After sterilization, the broth was inoculated with an overnight grown culture of *Escherichia coli*. Broth without inoculation was used as blank. To the broth M-12 and Ag decorated M-12 membrane's rectangular pieces (5 cm × 5 cm) were added and incubated in a rotary shaker at 37°C at 140 rpm for 24 h. Later the membrane pieces were removed and broth samples were diluted 5 times and optical density was analyzed at a wavelength of 600 nm using UV-Vis spectroscopy.

4. Results and discussion

4.1. Characterization of amine functionalized TiO_2 nanoparticles

As seen from the TEM images in Fig. 3, functionalized TiO_2 nanoparticles had an average diameter of around 25–30 nm. By comparing the TEM images of ATNP and TNP it is clear that functionalization has not affected the size of the nanoparticles. Since functionalization takes place only at the surface of the nanoparticle [22].

In the Fig. 4, FTIR spectrum of the TNP and ATNP is compared. Due to the presence of physisorbed water, the O-H bonds in Ti-OH groups vibrate, which is represented by the peak around 1627 cm^{-1} and the broad peak around 3300–3400 cm^{-1}. The lowering of transmittance beyond 900 cm^{-1} corresponds to the longitudinal optical mode of anatase phase and also to Ti-O-Ti bonds [25]. The FTIR spectra of ATNP show some striking deviations from that of TNP. The presence of amine groups on the surface of TiO_2 functionalized nanoparticles are represented by the peak at 1616 cm^{-1} which corresponds to N-H bond. XRD Peaks around 25.4°, 38.5°, 48° and 53.8° in the ATNP confirms the anatase phase of TNP (Fig.7) [26].

4.2. Characterization of silver nanoparticle suspension

Silver nanoparticle suspension was reddish brown in color and showed a peak at 440 nm in UV-Vis spectra (Fig. 5). The presence of peak between 420–450 nm corresponds to the characteristic surface plasmon of silver nanoparticles and therefore confirms the nanosize of particles [27]. The color of silver nanoparticles is dependent on the size. When compared with literature the peak at 440 nm corresponds to a particle size of 50 nm [28].

4.3. Membrane characterization

4.3.1. FT-IR Analysis

Comparison of FTIR spectra of M-0, M-12 and ATNP is shown in Fig. 6. M-0 membrane is a blend of PSF and CA.

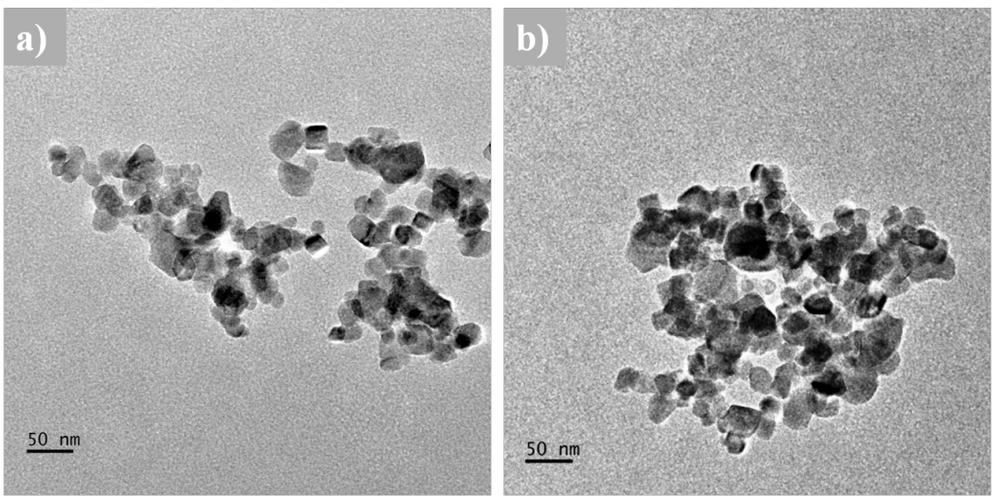

Fig. 3. TEM image of a) ATNP b) TNP.

The peaks at 1293 cm^{-1}, 1240 cm^{-1} , 1150 cm^{-1} of the M-0 represents S=O asymmetric stretch, C-O-C stretch, S=O symmetric stretch of PSF [29]. CA peaks at 2939 cm^{-1} and 2871 cm^{-1} corresponding to the asymmetric and symmetric C-H stretching, 1744 cm^{-1} (C=O stretching), 1168 cm^{-1} (asymmetric stretching of the C–O–C bridge) and 1215 cm^{-1} (carboxylate C-O stretch) is also seen [30]. These peaks can also be seen for the hybrid membrane M-12 as well. Significant deviation in transmittance is seen for the hybrid membrane due to effect of ATNP addition. The elevation of transmittance around 1140 cm^{-1} and the lowering of transmittance 2360 cm^{-1} point to the merger of ATNP and polymer peaks, indicating good additive polymer interaction.

4.3.2. XRD analysis

Comparison of the XRD pattern of ATNP, M-0, M-12 is done in Fig. 7. XRD of M-0 shows only a single broad peak around 18.3° which corresponds to the amorphous peak of CA. In M-12 membrane, the characteristic peaks of anatase can be clearly seen although at a lower intensity. The amorphous peak of CA at 18.3° has become more dominant. The emergence of crystalline peak of CA at 14.9° indicates that addition of ATNP has result in formation of crystalline CA during phase inversion [31]. There is a diminutive shift in the peaks which shows effective incorporation and good interaction between filler and matrix.

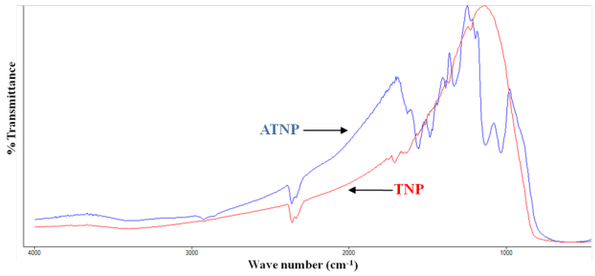

Fig. 4. FT-IR spectrum a) ATNP and b) TNP.

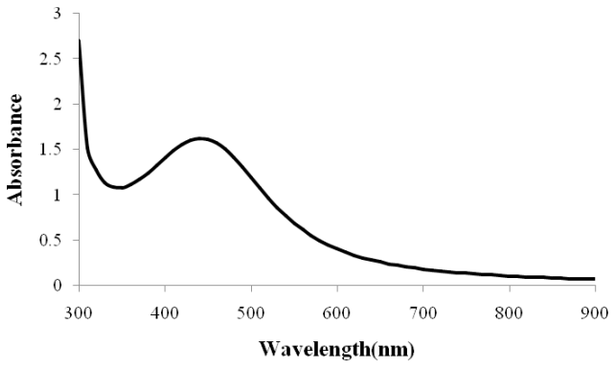

Fig. 5. UV-Vis spectra of silver nanoparticle suspension.

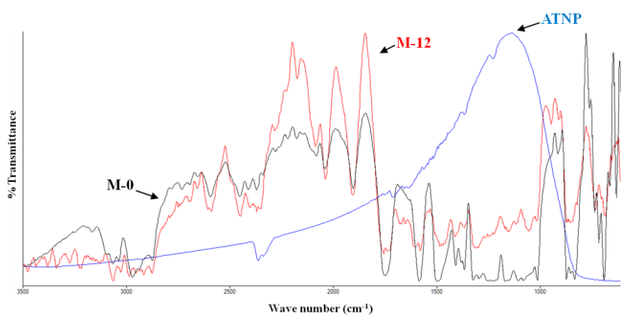

Fig. 6. FT-IR spectra of ATNP, M-0, and M-12.

4.3.3. SEM analysis of the membranes

The SEM analysis of the cross-sectional view of the membranes are displayed in Fig. 8, where finger-like structures usually found under the skin layer of UF membranes sub structure, the medium sized macrovoids extending through one-third of the membrane, and the small macro voids are situated near the nodular layer. The skin becomes porous and sponge structure is observed along the bottom of the penetrating cavity. As ATNP concentration is increased, the macro pores start to change [32]. The finger like projections became shorter [33]. An increased spongy layer formation is also observed at higher additive content.

SEM surface image of M-12 membrane clearly shows the presence of numerous silver nanoparticles bonded on to the membrane surface (Fig. 8h). SEM elemental maps of Ag on the membrane surface also revealed that good number of nanoparticles had adsorbed on to the membrane surface (Fig. 9).

4.3.4. Hydrophilicity of membranes

Hydrophilicity of the membranes active surface plays an important role to establish the membrane flux and antifouling properties. The hydrophilicity of the membrane can be studied using contact angle measurement. Fig. 10 shows the contact angle measurements of the membranes. There was a gradual decrease in the contact angle of the membranes from 89.42° for M-0 to 44.11° for M-12. A considerable decrease in the contact angle occurred when the concentration of ATNP was increased; this shows that hydrophilicity of the membranes was enhanced with addition of ATNP [34].

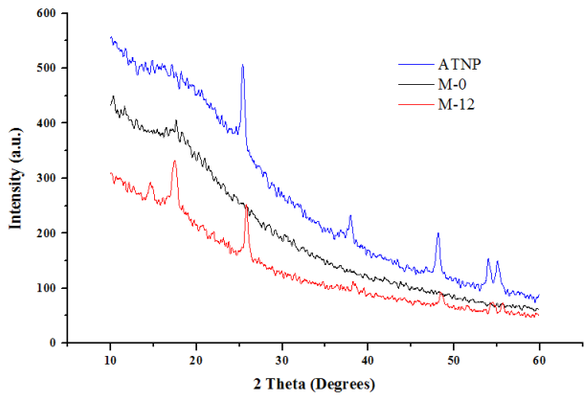

Fig. 7. XRD patterns of M-0, M-12, and ATNP.

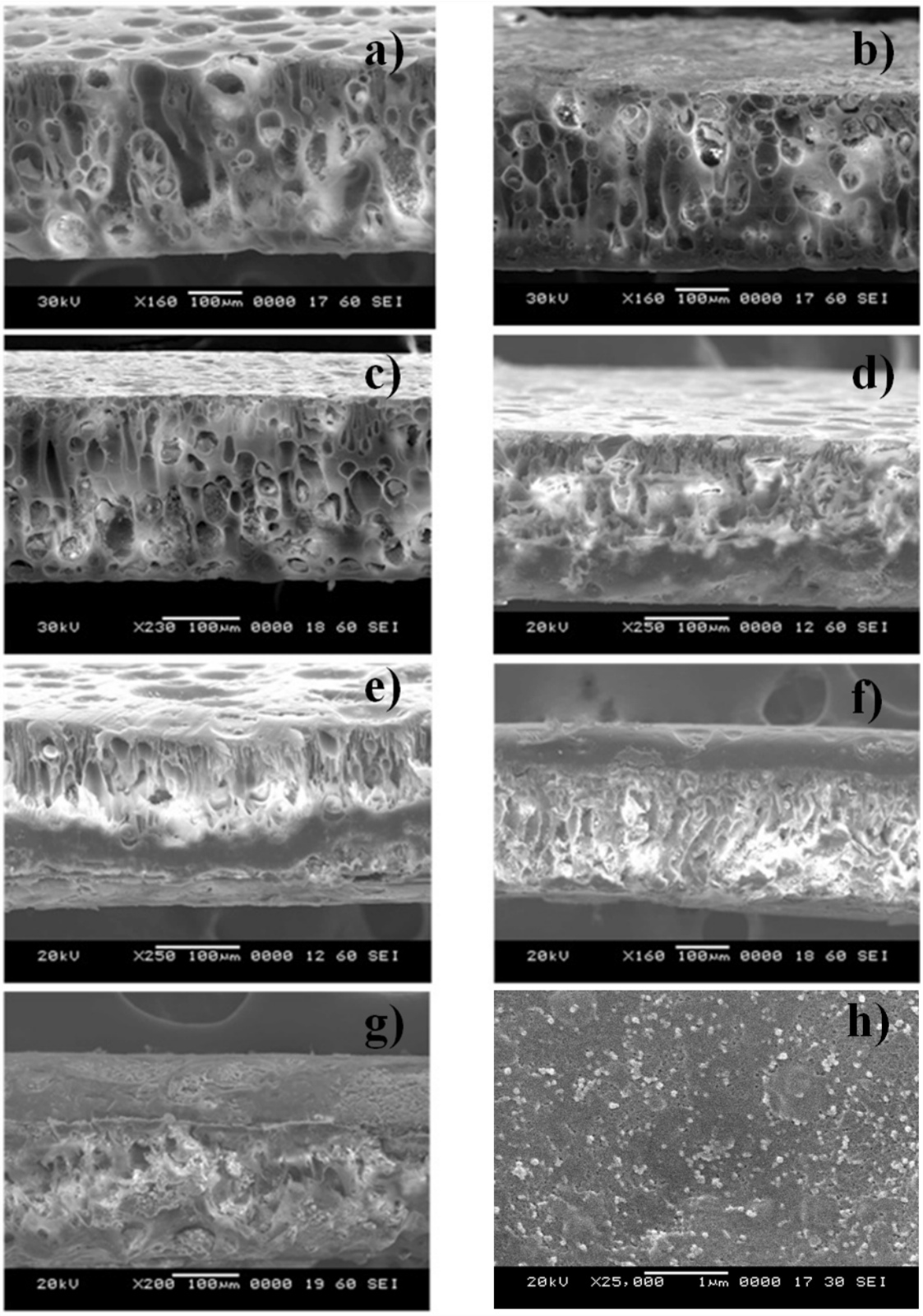

Fig. 8. Cross-sectional SEM images of membranes. (a) M-0; (b) M-1; (c) M-3; (d) M-5; (e) M-7; (f) M-10; (g) M-12; (h) Surface image of M-12.

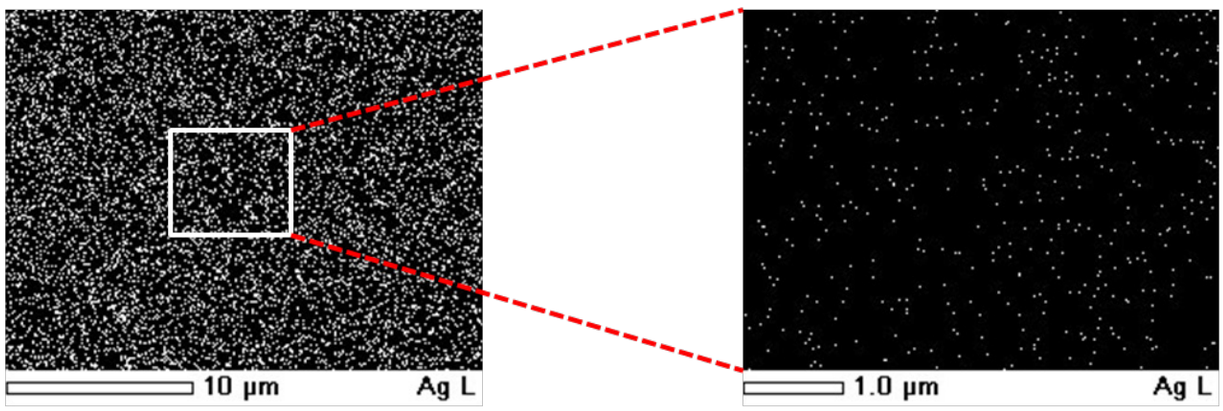

Fig. 9. SEM elemental maps of Silver (Ag) nanoparticles on M-12 membrane surface.

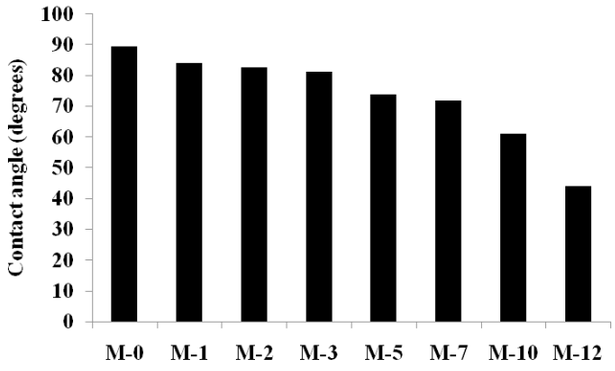

Fig. 10. Contact angle measurements of the membranes.

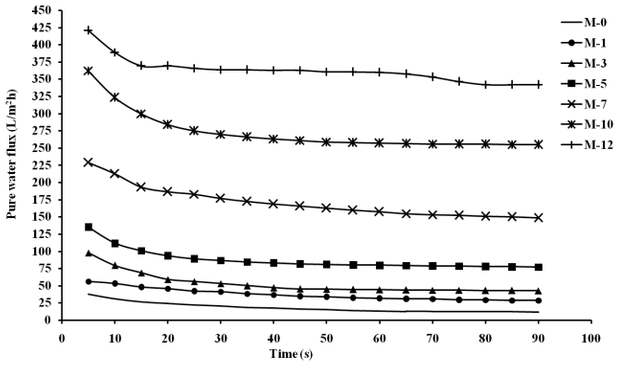

Fig. 11. The PWF of the membranes.

4.3.5. Membrane permeability and antifouling properties

Permeation characteristics of the membrane were accessed in terms of pure water flux at 0.2 MPa and 25°C. Initially the membranes showed steep flux drop due to mechanical compaction [35]. After a while of pressurization the flux decline gradually decreased. The flux values are given in Fig. 11. It was evident that the membranes showed a drastic increase in flux when compared to the nascent membrane with increasing ATNP content. The maximum flux was seen in case of 12% addition of ATNP.

Rejections of the membranes were estimated using BSA as a standard protein. The trends of flux during rejection studies are given in Fig. 12. The BSA rejection values of M-0, M-1, M-3, M-5, M-7, M-10, M-12 membranes were 94.44%, 93.81%, 92.44%, 91.74%, 91.98%, 94.54%, 92.61%, respectively. All membranes showed drastic flux drop from the PWF values during rejection study. As seen in case of PWF studies the hybrid membranes showed better flux during BSA rejection. Maximum flux was obtained for M-12 membrane.

The antifouling properties of the membranes were evaluated in terms of flux recovery ratio (FRR). As shown in Fig. 13, all hybrid membranes showed better flux recovery than the nascent M-0 membrane. The best recovery was seen in case of M-12 membrane, 78.36%.

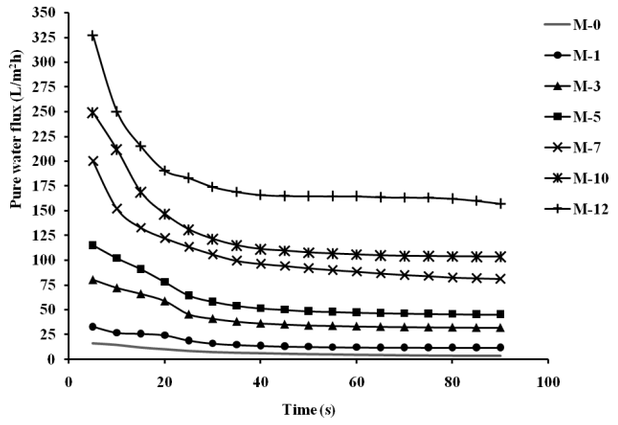

Fig. 12. The membrane fluxes during BSA rejection.

4.3.6. Antibacterial properties

After one day of incubation, the zone of inhibition results of Ag decorated and undecorated M-12 membranes obtained are shown in the Fig. 14. The Ag decorated membrane showed a very clear zone of inhibition [36]. No bacterial growth was seen on the membrane

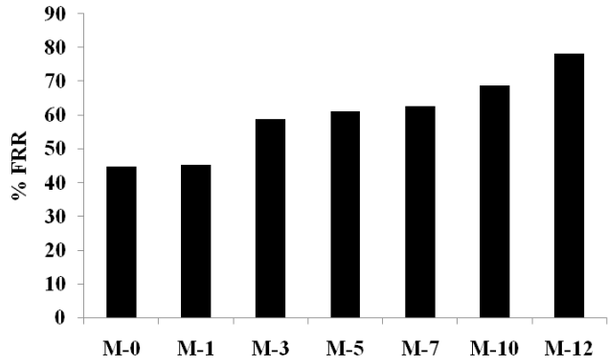

Fig. 13. Percentage flux recovery ratio of the membranes.

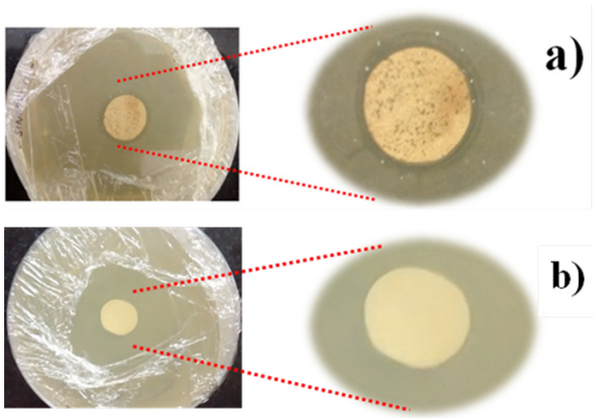

Fig. 14. Zone of inhibition results a) Ag decorated M-12 membrane b) control.

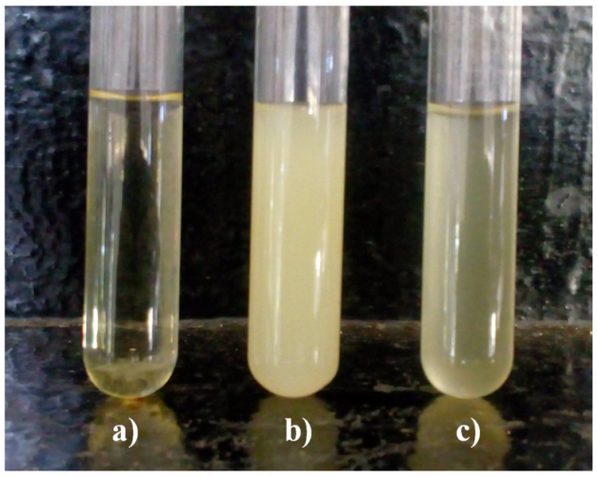

Fig. 15. Turbidity of broth with a) no microbial addition b) M-12 membrane c) Ag decorated M-12 membrane.

surface as well, indicating that the membranes had bacterial resistance due to the presence of silver. Whereas for undecorated membranes no zone of inhibition is observed. The bacteria were able to grow on the membrane surface as well.

Table 2
Optical density of culture media

Sample	Optical density
Broth	0.038
M-12	0.824
Ag decorated M-12	0.148

Antibacterial properties of the Ag decorated membrane in liquid media were evaluated and the results are shown in Fig. 15. The optical density values of 5 time's diluted culture media are given in Table 2. The Ag decorated M-12 membrane showed very less growth in bacteria when compared to the high growth seen in case of undecorated membrane. Clearly indicate that Ag coating can hinder bacterial growth and prevent bio-fouling and film formation on the membrane surface.

5. Conclusions

Amine functionalized titanium oxide nanoparticles were successfully synthesized with diameters of 25–30 nm as observed from FTIR spectroscopy and TEM images. XRD confirmed that these nanoparticles were in anatase phase. Hybrid membranes with different compositions were synthesized with a maximum additive content of 12 wt%. Silver decoration of the membrane surfaces could be accomplished using the amine groups on nanoparticles, as seen from elemental maps. SEM images revealed asymmetric structure for all membranes, the spongy layer formation increased with increased additive content. Permeation studies showed high pure water flux and better flux retention during BSA rejection. The hybrids membranes showed enhanced antifouling properties due to the increased hydrophilicity. Antibacterial studies revealed the bactericidal effect of the Ag decorated membrane on *E. Coli*. In summary, a hybrid membrane with high water flux, better antifouling properties and antibacterial properties has been synthesized.

Acknowledgements

The authors thank Prof. K. Narayan Prabhu, Metallurgical and Materials Engineering Department of NITK Surathkal, India for providing contact angle measurement facility.

Symbols

J_w — Flux of pure water (L/m²h)
A — Cross section area of membrane (m²)
Q — Amount of permeate collected (L)
Δt — Time duration (h)
wt — Weight
FRR% — Flux recovery ratio (%)
R% — % BSA rejection
C_p — BSA concentrations in permeate (mg/mL)
C_f — BSA concentrations in feed (mg/mL)

References

[1] A. Urkiaga, D. Iturbe, J. Etxebarria, Effect of different additives on the fabrication of hydrophilic polysulfone ultrafiltration membranes, Desal. Water Treat., 56 (2015) 3415–3426.

[2] Y. Ma, F. Shi, J. Ma, M. Wu, J. Zhang, C. Gao, Effect of PEG additive on the morphology and performance of polysulfone ultrafiltration membranes, Desalination, 272 (2011) 51–58.

[3] M.K. Sinha, M.K. Purkait, Increase in hydrophilicity of polysulfone membrane using polyethylene glycol methyl ether, J. Membr. Sci., 437 (2013) 7–16.

[4] O. Kuttowy, S. Sourirajan, Cellulose acetate UF membranes, J. Appl. Polym. Sci., 19 (1975) 1449–1460.

[5] G. Arthanareeswaran, P. Thanikaivelan, K. Srinivasn, D. Mohan, M. Rajendran, Synthesis, characterization and thermal studies on cellulose acetate membranes with additive, Europe Polymer J., 40 (2004) 2153–2159.

[6] M. Sivakumar, D.R. Mohan, R. Rangarajan, Y. Tsujita, Studies on cellulose acetate-polysulfone ultrafiltration membranes: I. Effect of polymer composition, Polym. Int., 54 (2005) 956–962.

[7] M. Sivakumar, D.R. Mohan, R. Rangarajan, Studies on cellulose acetate-polysulfone ultrafiltration membranes: II. Effect of additive concentration, J. Membr. Sci., 268 (2006) 208–219.

[8] L. Yu, Y. Zhang, B. Zhang, J. Liu, H. Zhang, C. Song, Preparation and characterization of HPEI-GO/PES ultra filtration membrane with antifouling and antibacterial properties, J. Membr. Sci., 447 (2013) 452–462.

[9] Q. Zhao, J. Hou, J. Shen, J. Liu, Y. Zhang, Long-lasting antibacterial behavior of a novel mixed matrix water purification membrane, J. Mater. Chem. A., 3 (2015) 18696–18705.

[10] L. Duan, Y. Wang, Y. Zhang, J. Liu, Applied surface science graphene immobilized enzyme/polyethersulfone mixed matrix membrane: Enhanced antibacterial, permeable and mechanical properties, Appl. Surf. Sci., 355 (2015) 436–445.

[11] L. Duan, W. Huang, Y. Zhang, RSC Advances by facile blending with N-halamine grafted halloysite nanotubes, RSC Adv., 5 (2014) 6666–6674.

[12] A. Khalid, A.A. Al-Juhani, O.C. Al-Hamouz, T. Laoui, Z. Khan, M. Ali, Preparation and properties of nanocomposite polysulfone/multi-walled carbon nanotubes membranes for desalination, Desalination, 367 (2015) 134–144.

[13] J. Lee, H. Chae, Y. June, K. Lee, C. Lee, H.H. Lee, I. Kim, J. Lee, Graphene oxide nanoplatelets composite membrane with hydrophilic and antifouling properties for wastewater treatment, J. Membr. Sci., 448 (2013) 223–230.

[14] M. Prasad, S. Mohanty, S.K. Nayak, Study of polymeric nanocomposite membrane made from sulfonated polysulfone and nanoclay for fuel cell applications, High Perform. Polym., 26 (2014) 578–586.

[15] J. Dai, K. Xiao, H. Dong, W. Liao, X. Tang, Z. Zhang, S. Chai, Preparation of Al_2O_3/PU/PVDF composite membrane and performance comparison with PVDF membrane, PU/PVDF blending membrane, and Al_2O_3/PVDF hybrid membrane, Desal. Water Treat., 57 (2016) 487–494.

[16] M. Homayoonfal, M.R. Mehrnia, M. Shariaty-Niassar, A. Akbari, M.H. Sarrafzadeh, A. Fauzi Ismail, Fabrication of magnetic nanocomposite membrane for separation of organic contaminant from water, Desal. Water Treat., 54 (2015) 3603–3609.

[17] H. Yu, Y. Zhang, J. Zhang, H. Zhang, J. Liu, Preparation and antibacterial property of SiO_2–Ag/PES hybrid ultrafiltration membranes, Desalin. Water Treat., 51 (2013) 3584–3590.

[18] E. Yuliwati, Morphological and separation performance study of polysulfone/titanium dioxide (PSF/TiO_2) ultrafiltration membranes for humic acid removal, Desalination, 273 (2011) 85–92.

[19] Y. Yang, H. Zhang, P. Wang, Q. Zheng, The influence of nanosized TiO_2 fillers on the morphologies and properties of PSF UF membrane, J. Membr. Sci., 288 (2007) 231–238.

[20] A.K. Nair, P.E. Jagadeesh Babu, TiO_2 nanosheet-graphene oxide based photocatalytic hierarchical membrane for water purification, Surf. Coatings Technol., (2017) doi:10.1016/j.surfcoat.2017.01.022.

[21] R. Goei, T.T. Lim, Ag-decorated TiO_2 photocatalytic membrane with hierarchical architecture: Photocatalytic and antibacterial activities, Water Res., 59 (2014) 207–218.

[22] Z. Xu, S. Ye, G. Zhang, W. Li, C. Gao, C. Shen, Q. Meng, Antimicrobial polysulfone blended ultrafiltration membranes prepared with Ag/Cu_2O hybrid nanowires, J. Membr. Sci., 509 (2016) 83–93.

[23] Y. An, M. Chen, Q. Xue, W. Liu, Preparation and self-assembly of carboxylic acid-functionalized silica, J. Colloid Interface Sci., 311 (2007) 507–13.

[24] Y. Lv, H. Liu, Z. Wang, S. Liu, L. Hao, Y. Sang, D. Liu, J. Wang, R.I. Boughton, Silver nanoparticle-decorated porous ceramic composite for water treatment, J. Membr. Sci., 331 (2009) 50–56.

[25] M. Reza, H. Abdizadeh, Effects of acid catalyst type on structural, morphological, and optoelectrical properties of spin-coated TiO_2 thin film, Phys. B Phys. Condens. Matter, 413 (2013) 40–46.

[26] A. Zaleska, E. Kowalska, T. Klimczuk, TiO_2 photoactivity in vis and UV light: The influence of calcinations temperature and surface properties, Appl. Catal. B, 84 (2008) 440–447.

[27] G.A. Martinez-Castanon, N. Niño-Martínez, F. Martínez-Gutierrez, J.R. Martínez-Mendoza, F. Ruiz, Synthesis and antibacterial activity of silver nanoparticles with different sizes, J. Nanoparticle Res., 10 (2008) 1343–1348.

[28] S. Agnihotri, S. Mukherji, S. Mukherji, Size-controlled silver nanoparticles synthesized over the range 5–100 nm using the same protocol and their antibacterial efficacy, RSC Adv., 4 (2014) 3974.

[29] A.K. Nair, P.M. Shalin, P.E. Jagadeesh Babu, Performance enhancement of polysulfone ultrafiltration membrane using TiO_2 nanofibers, Desal. Water Treat., 57 (2016) 10506–10514.

[30] C.H. Worthley, K.T. Constantopoulos, M. Ginic-Markovic, E. Markovic, S. Clarke, A study into the effect of POSS nanoparticles on cellulose acetate membranes, J. Membr. Sci., 431 (2013) 62–71.

[31] A.S. Abdel-Naby, A.A. Al-Ghamdi, Chemical modification of Cellulose Acetate by Diallylamine, Int. J. Curr. Microbiol. App. Sci., 3 (2014) 10–24.

[32] B. Singh, V. Kochkodan, R. Hashaikeh, N. Hilal, A review on membrane fabrication : Structure, properties and performance relationship, Desalination, 326 (2013) 77–95.

[33] V.E. Reinsch, A.R. Greenberg, S.S. Kelley, R. Peterson, L.J. Bond, A new technique for the simultaneous, real-time measurement of membrane compaction and performance during exposure to high-pressure gas, J. Membr. Sci., 171 (2000) 217–228.

[34] C. Dong, G. He, H. Li, R. Zhao, Y. Han, Y. Deng, Antifouling enhancement of poly (vinylidene fluoride) microfiltration membrane by adding $Mg(OH)_2$ nanoparticles, J. Membr. Sci., 387–388 (2012) 40–47.

[35] S.B. Teli, S. Molina, E.G. Calvo, A.E. Lozano, J. de Abajo, Preparation, characterization and antifouling property of polyethersulfone–PANI/PMA ultrafiltration membranes, Desalination, 299 (2012) 113–122.

[36] J. Li, X. Shao, Q. Zhou, M. Li, Q. Zhang, The double effects of silver nanoparticles on the PVDF membrane : Surface hydrophilicity and antifouling performance, Appl. Surface Sci., 265 (2013) 663–670.